

Dong, B., Xie, D., He, F., & Huang, L. (2021). Noise attenuation and performance study of a small-sized contra-rotating fan with microperforated casing treatments. *Mechanical Systems and Signal Processing*, 147, 107086.

doi:<https://doi.org/10.1016/j.ymssp.2020.107086>

**Noise attenuation and performance study of a small-sized contra-rotating fan with microperforated casing treatments**

Bin Dong<sup>a,b,d,\*</sup>

Dan Xie<sup>c,e</sup>

Fan He<sup>a</sup>

Lixi Huang<sup>b,d</sup>

<sup>a</sup>High Speed Aerodynamics Institute, China Aerodynamics Research and Development Center, No.6, South Section, Second Ring Road, Mianyang, Sichuan, China, 621000.

<sup>b</sup>Department of Mechanical Engineering, The University of Hong Kong, Pokfulam Road, Hong Kong SAR, China.

<sup>c</sup>College of Astronautics, Northwestern Polytechnical University, Xi'an, Shaanxi, China, 710072.

<sup>d</sup>Laboratory for Aerodynamics and Acoustics, Zhejiang Institute of Research and Innovation, The University of Hong Kong, Hong Kong SAR, China.

<sup>e</sup>Department of Mechanical Engineering, The Hong Kong Polytechnic University, Hong Kong SAR, China

Corresponding author: Bin Dong, High Speed Aerodynamics Institute, China Aerodynamics Research and Development Center, No.6, South Section, Second Ring Road, Mianyang, Sichuan, China

E-mail: [irendong@connect.hku.hk](mailto:irendong@connect.hku.hk)

Submitted to *Mechanical Systems and Signal Processing* February 21 2020

Accepted June 19 2020

### Author Biographies

Bin Dong was a PhD student at the University of Hong Kong. His research interests are in aerodynamic noise and fluid dynamics.

Dan Xie, PhD, is Professor at Northwestern Polytechnical University. Her research interests are in aeroelastic mechanics, nonlinear dynamics and modal reduction techniques for high-dimensional models.

Fan He,

Lixi Huang

## Noise attenuation and performance study of a small-sized contra-rotating fan with microperforated casing treatments

### Abstract:

This study investigates the benefits of noise control for a small-sized contra-rotating (CR) fan using microperforated-panel (MPP) casing treatments over the rotor. Several configurations of this type of casing treatment were proposed and then simulated with the finite element method (FEM) to determine their acoustic performance. In general, the FEM simulations indicated that the configurations of placing the treatment over the front rotor are more acoustically effective than those over the rear rotor. Experimentally, it was found that each axial row of holes of the MPP casing behaves like a stator vane, interacting with the fan rotor and thus generating a noisy interaction tone. However, such a tone can be sufficiently suppressed by optimizing the row numbers at the design stage of the MPP casing to increase the interaction mode and frequency. Experimental results further showed that for the treatment over the front rotor, the fan performance was not significantly influenced, especially in the flow rate region above stall point, while for the treatment over the rear rotor, a pressure loss of no more than 10 Pa was perceived, particularly in the flow rate region around the fan design point. Acoustically, the former was able to reduce overall noise throughout the flow rate region, with a maximum noise reduction of 3.5 dBA around the design point, whereas the latter increased overall noise slightly. Moreover, an enlarged volume lowering cavity stiffness for the treatment over the front rotor was found to improve the reduction of overall noise by 0.7 dBA (from 2.8 dBA to 3.5 dBA) as well as to attenuate rotor-alone tones effectively, of which the front treatment with the regular cavity failed in noise reduction. In contrast, no substantial enhancements of noise reduction were noticed for the rear treatment with an enlarged cavity. It is anticipated that the current investigation can provide a reference for controlling CR fan noise with MPP casing treatments.

(314 words)

**Keywords:** contra-rotating fan; noise attenuation; microperforated-panel casing treatment; finite element method; casing-rotor interaction; performance study.

## 1 Introduction

There is a growing interest in developing contra-rotating (CR) fans as a potential alternative to equivalent turbofans due to less specific fuel consumption and lower emission of greenhouse gas [1-3]. In general, a CR fan comprises two rotors enclosed within a casing that rotate in opposite directions around the same axis. The advantage lies in the fact that the rear rotor is able to not only recover the residual swirl from the front rotor but also transfer energy to the working fluid directly, which can make significant improvements in the propulsion efficiency or thrust compared to the single-rotor fan. However, a crucial problem arises that the wake-rotor interaction, the tip-vortex interaction, and the potential-field interaction between front and rear rotors tend to generate high-level noise radiation [1]. Such induced radiation would possibly breach environmental requirements concerning noise emission. It is, therefore, of central importance to reduce noise radiation from CR fans for better performance in practical applications (e.g., turbofans, ventilators, and cooling fans). In principle, the noise radiated by a fan (hereinafter, fan noise) is an inevitable by-product of its energy-transfer process, which consists of a series of discrete tones superimposed on a broadband bottom. The tones are usually attributed to the rotor rotational speed, while the broadband bottom is related to random vortices, which can be contained in the boundary layers of the blades or enclosures, the tip leakage flow, or the wakes shed from blade trailing edges. Fan noise is unwanted for most cases, so it should be adequately minimized. A variety of methods have been devised and can be found in the open literature, such as mismatching blade count, using scarf inlet, applying the acoustic liner, sweeping the blade profile, perforating the blade trailing edge, etc. [4-6]. Among these methods, the acoustic liner is probably most widely used because of its effectiveness and robustness over a broad range of frequencies and an easy integration with other fan components. The liner is able to not only provide acoustic absorption when sound propagates along the liner but also present a pressure release boundary condition when it is installed near the acoustic source, thus mitigating the acoustic near field and reducing the far-field noise. Many efforts have been made in applying the acoustic liner to attenuate fan noise, and a selected few of them will be mentioned below.

Khorrami et al. [7] investigated, through steady computational simulations, the feasibility of positively modifying the tip-clearance flowfield of a compressor cascade. They demonstrated that substantial noise attenuation was achieved because the formation of the tip vortex was delayed by moving the tip vortex trajectory away from the blade tip edge. Additionally, the intensity of the tip

vortex, the shear layer rollup, and the boundary layer separation were all reduced. Sutliff and Jones [8] installed a foam-metal liner close to the rotor for noise attenuation of a low-speed fan. In comparison to the traditional liner placed in the fan inlet or exhaust nacelle, the foam-metal liner had the potential to reduce fan noise by 4 dB due to the fact that the acoustic near field was positively modified, thus impairing the noise-generation mechanism. Sutliff and Jones [9] continued to study the effectiveness of applying foam-metal liners to a high-speed fan. They observed that foam-metal liners were most effective below sonic fan tip speed, and significant noise reductions of up to 5 dB could be achieved with a marginal influence on fan aerodynamic performance. The potential of using acoustic splitters made of microperforated panels (MPPs) in the inlet or outlet to control cooling fan noise was studied by Allam and Abom [10]. They proposed theoretical models to quantify the acoustic energy attenuation and the transmission loss by the splitters and concluded that the MPP splitter should be made more locally reacting for a higher transmission loss. Recently, an MPP housing device was introduced to a small-sized axial flow fan for controlling the tones at the first two blade passing frequencies (BPFs), for which effective sound absorption was noted [11]. Similarly, aiming at reducing the blade passage tone level of an axial flow fan, Lee and Bolton [12] incorporated MPPs into the housing around the fan circumference and succeeded in attenuating the tone level up to 2.5 dBA. Wang et al. [13] applied the MPP housing integrated with a Herschel-Quincke tube to control noise radiation from an axial flow fan. Their theoretical and experimental results showed that the integrated configuration possessed a dominating performance of suppressing noise over the conventional MPP housing due to the combined effects of vibroacoustic coupling, micro-perforation absorption, and Herschel-Quincke interference. Nevertheless, in their simulations modeling the axial flow fan as a simple dipole in the axial direction neglects the influences of the fan structures on noise radiation, and thus may lose some acoustic features.

The studies cited above provide us a strong foundation for grasping knowledge about how to attenuate fan noise using acoustic liners constructed of different materials, such as metal foam and MPPs. Unlike large-sized or high-speed fans that can be frequently found in the aviation industry, small-sized fans are classically incompressible turbomachines often used as air coolers or ventilators in heating, ventilation, and air conditioning (HVAC) systems. In practice, when a higher pressure rise or a larger volumetric flow rate is needed in some HVAC systems, small-sized fans can be arranged to work in series or parallel, respectively. A higher pressure rise is

advantageous to overcome the system resistance, and a larger flow rate can take away more heat through airflow. However, since fans in series and parallel are rotating separately instead of being aerodynamically coupled, the combined efficiency would be lower, thereby consuming more energy. Moreover, series or parallel operation is usually not able to achieve a higher pressure rise and a larger volumetric flow rate simultaneously, in which the CR fans are specialized and can be used to replace the traditional fans. For practical applications in HVAC systems, as fans are normally installed in close vicinity to places where people live and work, it is necessary to reduce their noise annoyance for a quieter environment. The acoustic liner, due to its easy integration with fan structures, can be used for noise reduction. In the present work, the liner is installed over the front and rear rotors of a small-sized CR fan. It should be noted that for large-sized fans in the aviation industry, the acoustic liner is generally placed in the inlet and exhaust nacelle rather than over the fan rotor, which is a much harsher pressure and temperature environment. If designed correctly with proper materials and structures, such as metal-foam layers with and without a perforated face sheet, the liner can also be placed over the rotor in large-sized fans [8-9, 14-15]. However, the problem with increased air jetting through foam pores and metal foam impingement onto the blade surface could arise due to the harsh environment over the rotor in large-sized fans. For a small CR fan that works at low speeds (incompressible flow), the environment over the rotor is more benign, thereby relieving the problem. In this environment, the MPP liner with a thin face sheet can be applied, which can be designed to provide the required acoustic properties to achieve the desired surface impedance for noise reduction without using bulk-reacting porous materials. In the literature, there is not much attention paid to assessing the effect of MPP casing treatments on noise reduction and aerodynamic performance of small-sized CR fans, which therefore becomes the focus of the current study.

At first, an acoustically effective liner was designed based on the averaged spectrum of a small-sized CR fan working at the design point, where the key was to overcome the acoustic interaction between the MPP casing and the rotor (hereinafter, casing-rotor interaction). The performance characteristics of the MPP casing were then investigated acoustically and aerodynamically as a function of the volumetric flow rate. Finally, the potential impacts of placing the MPP casing over the front and rear rotors on noise attenuation at the fan design point were examined in detail. The underlying mechanisms of these impacts were also proposed in order to give a better insight into the physical process of CR fan noise control via microperforated liners.

The layout of this paper is as follows. In § 2, experimental preparations related to the testing CR fan (§§ 2.1) and the acoustic measurement (§§ 2.2) are presented. Then, the design process of an acoustically effective MPP casing is documented in § 3. More specifically, in §§ 3.1, acoustic performance prediction of the MPP casing is treated using the impedance model proposed by Allam and Abom [16]. In §§ 3.2, the performance prediction is further validated by performing three-dimensional (3D) simulations with the finite element method (FEM), followed by the investigation of casing-rotor interaction in §§ 3.3. The treatment configurations tested in experiments are summarized in § 4. The acoustic benefits achieved by the MPP treatments, as well as their impacts on fan aerodynamic performance, are reported in § 5. Finally, some conclusions are drawn in § 6.

## 2 Experimental preparations

### 2.1 The testing contra-rotating fan

A small-sized CR fan with low tip speed ( $U_t \approx 20\text{m/s}$ ) designed in Refs. [3] is utilized as an experimental subject. The testing fan is expected to generate  $4.0 \text{ m}^3/\text{min}$  airflow with a 150 Pa total pressure rise. The front and rear rotors have the same tip radius  $r_t = 57.2\text{mm}$  and hub radius  $r_h = 31.5\text{mm}$ . There are 7 and 5 blades in the front and rear rotors, denoted as  $B_1 = 7$  and  $B_2 = 5$ , respectively. The interstage axial spacing  $\eta_a$  between the front blade trailing edge and the rear blade leading edge is 18.2mm approximately. The radius  $r_d$  of the circular flow passage is 116mm, thereby leading to a tip clearance  $\varepsilon$  of 0.8mm. At the fan design point, the front rotor rotates at an angular speed of  $\Omega_1 = 3645 \text{ rpm}$  (revolutions per minute) and the rear rotor at  $\Omega_2 = 3165 \text{ rpm}$ . The rotational speeds are monitored by a tachometer.

### 2.2 The acoustic measurement

The noise signals from the test fan are measured in a fully anechoic chamber, which provides an anechoic environment down to a frequency of 100 Hz. The fan is placed at the inlet of an aerodynamic test rig used to measure the volumetric flow rate and the total pressure rise of the fan. Figure 1 presents the setup of acoustic measurement. A B&K Nexus conditioning amplifier is applied to power four 1/4-inch microphones, which are evenly distributed along a quarter-circle at four angular positions located 0.8m horizontally away from the center of the front rotor. A 16-bit A/D card (NI USB-6251) is employed to sample noise data at a frequency of 51.2 kHz, and the

duration for each data acquisition is set to be 20 seconds. Signal processing is then conducted on a personal computer installed with the software MATLAB. The averaged sound spectrum is obtained by averaging the spectra from the four angular positions. Furthermore, during the processing, A-weighting values are added to the measured sound pressure level (SPL in dB re. 20  $\mu$ Pa) in order to account for the relative loudness perceived by the human ear, as the ear is less sensitive to low audio frequencies. The A-weighted SPL is abbreviated as SPLA in dBA.

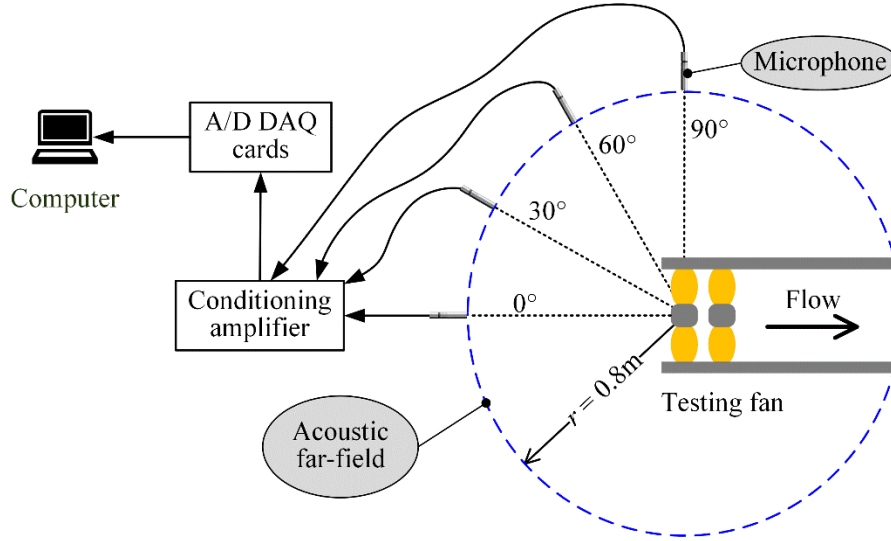


Fig. 1. The setup of acoustic measurement in the anechoic chamber.

### 3 Design of the MPP casing

In practice, the fan is capable of working in a broad operating range, spanning from the low flow rate region to the high flow rate region. However, it is, in the close vicinity of the design point, that the fan typically has a better aerodynamic performance over other operating points, and therefore a relatively lower noise level. Hence, we choose the averaged spectrum of the testing fan working at the design point to determine the MPP casing acoustic parameters. Also, casing-rotor interaction will be addressed based on the theory of stator-rotor interaction [17].

#### 3.1 Spectral analysis of CR fan noise

The averaged spectrum of the testing fan working at the design point within hard-wall casings is illustrated in Fig. 2a, where the prominent tones larger than 35 dBA are marked with black dots (•). The curve is plotted on a logarithmic scale with a resolution of the 1/48 octave band. The front and rear rotor BPFs are denoted as  $f_1$  and  $f_2$ , respectively. These tones are all related to the rotor-



alone tone and the interaction tone. The former is composed of integer multiples of either  $f_1$  or  $f_2$ , while the latter depends upon the linear combinations of  $f_1$  and  $f_2$ . The overall noise level (integrated over the frequencies from 20 to 8000 Hz) of the testing fan at the design point is 61.5 dBA. The averaged spectrum is plotted in SPLA, which is not a useful tool to demonstrate acoustic energy distribution over frequencies or the intensity of a tone embedded in the spectrum. In this regard, the cumulative sound power (CSP) spectrum can be applied. In this study, the CSP spectrum is further normalized by the power of the overall noise level, as shown in Fig. 2b. In can be seen that the prominent tones distribute in the frequency band from 500 Hz to 2500 Hz. In total, there are two rotor-alone tones at the second and third harmonics of  $f_2$ , and four interaction tones with mode orders  $|m| \leq 3$ .

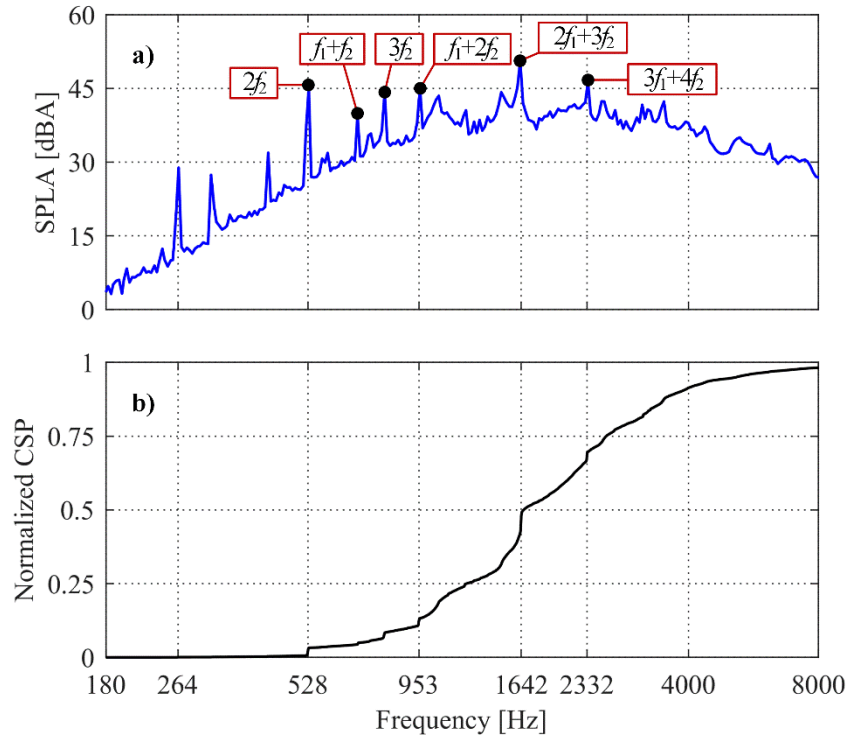


Fig. 2. Noise spectra of the testing fan; a) the averaged spectrum, and b) the normalized CSP spectrum.

The interaction frequency  $f_{in}$  and the circumferential mode order  $m$  of the prominent tones can be determined as [3, 18]

$$f_{in} = \frac{1}{60} |m_1 B_1 \Omega_1 + m_2 B_2 \Omega_2| \quad \text{and} \quad m = m_2 B_2 - m_1 B_1, \quad (1a, b)$$

where  $m_1$  and  $m_2$  are integers taking values from  $-\infty$  to  $+\infty$ . The sign of indices  $m_1$  and  $m_2$  must be the same, for which the mode of order  $m$  at a frequency  $f_{in}$  has an angular velocity that is much bigger than the equivalent velocity  $\Omega_e = \Omega_1 + \Omega_2$ , making the mode radiate efficiently. In contrast, when  $m_1$  and  $m_2$  are of opposite sign, the mode will rotate at a speed that is less than  $\Omega_e$ , thereby radiating weakly. Table 1 lists both the frequencies, mode orders, and noise levels of the prominent tones. The reason why the rotor-alone tones at  $2f_2$  and  $3f_2$  with higher orders present relatively higher noise levels is due to inflow distortion or strut-rotor interaction [3].

**Table 1.** The prominent tones with noise levels above 35 dBA

Frequency	$2f_2$	$f_1+f_2$	$3f_2$	$f_1+2f_2$	$2f_1+3f_2$	$3f_1+4f_2$
$f_{in}$ (Hz)	528	690	792	953	1642	2332
Order $m$	10	-2	15	3	1	-1
SPLA (dBA)	40.8	35.9	37.8	39.9	42.6	38.6

Figure 2b shows that the acoustic energy is fractionally contained in the frequency band below 953 Hz, only around 11%. After that, the curve begins to climb up sharply until 1642 Hz, where a steep step can be found, meaning that the intensity of the tone here is strong. The energy portion involved in this band is almost 39%, being more than three times that of the previous band. Subsequently, in the band from 1642 Hz to 2332 Hz, a relatively moderate rate of energy growth is observable, occupying about 20% of the total energy. Above 2332 Hz, there are no significant tones exhibited along the curve, implying that energy accumulation comes from broadband noise. In general, nearly 60% of the total acoustic energy is found to be contained in the band from 953 Hz to 2332 Hz. Therefore, the MPP casing treatment should be effective in sound absorption in this band. In particular, the acoustic energy is concentrated around the tone at 1642 Hz in the spectrum, suggesting that the peak absorption of the MPP casing should be designed near this tone. These spectral analyses can be used to determine the acoustic parameters of the MPP casing.

### 3.2 Acoustic parameters of the MPP casing

In practice, an MPP consists of a sheet panel with a lattice of sub-millimeter perforations spread over its surface. The sub-millimeter holes provide acoustic resistance and low acoustic mass reactance necessary for the absorber without using bulk-reacting porous materials, which may be harmful to human health, especially when they are applied in ventilation and air-conditioning systems [19, 20]. It appears that Maa [21] was the first researcher to present the idea

of the MPP absorber and proposed a classic model quantifying its impedance. The model is mainly intended for room acoustics and can be used as a design tool for panel absorbers. However, for those practical applications containing a steady flow, the classic model may become inaccurate due to the neglect of flow effects on the MPP acoustic impedance and, therefore, on sound absorption performance. In order to study such effects, Allam and Abom [16] have proposed a new model of perforate impedance, which shows good agreement with their experimental data measured using a newly developed technique [22]. Based on their model, the MPP impedance with a back cavity can be expressed as  $Z = Z_r + iZ_i$ , where the resistance  $Z_r$  is

$$Z_r = \text{Re} \left( \frac{ikt}{\sigma} \left( 1 - \frac{2J_1(\gamma\sqrt{-i})}{\gamma\sqrt{-i}J_0(\gamma\sqrt{-i})} \right)^{-1} \right) + \frac{4}{\sigma} \sqrt{\frac{\mu k}{2\rho_0 c_0}} + 0.15 \frac{M_g}{\sigma}, \quad (2a)$$

and the reactance  $Z_i$  takes the form of

$$Z_i = \text{Im} \left( \frac{ikt}{\sigma} \left( 1 - \frac{2J_1(\gamma\sqrt{-i})}{\gamma\sqrt{-i}J_0(\gamma\sqrt{-i})} \right)^{-1} \right) + 0.85 \frac{kdF_\delta}{\sigma} - \cot(kD). \quad (2b)$$

In the above equations,  $F_\delta = [1 + (12.6 \cdot M_g)^3]^{-1}$  represents the flow effect on reactance,  $M_g$  is the grazing flow Mach number,  $d$  is the hole diameter,  $t$  is the panel thickness,  $D$  is the depth of the back cavity,  $\sigma$  is the perforation ratio, and  $J_0$  and  $J_1$  are the Bessel functions of the first kind of zeroth and first order, respectively. The ambient air has dynamic viscosity  $\mu$ , mean density  $\rho_0$ , and speed of sound  $c_0$ . The fundamental wavenumber is  $k = 2\pi f/c_0$ , and the ratio of hole diameter to the viscous boundary layer thickness is defined as  $\gamma = d\sqrt{k\rho_0 c_0/4\mu}$ . The grazing mean flow is observed to increase resistance and decrease reactance [16, 23]. The ideal MPP behavior in terms of sound absorption can be determined using  $Z_r$  and  $Z_i$  as a coefficient  $\alpha$

$$\alpha = \frac{4Z_r}{(1 + Z_r)^2 + (Z_i)^2}. \quad (3)$$

Equation (3) shows that perfect or maximum absorption ( $\alpha = 1$ ) occurs when  $Z_r = 1$  and  $Z_i = 0$ , meaning pure resistance and no reactance. In the current work, in order to meet the requirement for sound absorption given by the spectral analysis in §§ 3.1, the proposed acoustic parameters are defined as  $d = 0.8$  mm,  $t = 1$  mm,  $\sigma = 4.95\%$  and  $D = 22$  mm. The mean flow through the fan stage is about 10m/s, leading to a grazing Mach number  $M_g$  of 0.03. Therefore, the convective effects on sound propagation can be neglected in comparison to the effects on the MPP impedance. A

Mach number of  $M_g = 0.03$  leads to a correction of 0.09 added to the resistance and  $F_\delta = 0.95$  for the reactance. The peak performance with an absorption coefficient of 0.63 happens at 1750 Hz, which is 100 Hz higher than the strongest tone at 1642 Hz (see Table 1). However, the absorption coefficient is still above 0.5, slightly lower than the peak coefficient, and therefore the strongest tone could be effectively controlled. Note that a relatively larger diameter ( $d = 0.8\text{mm}$ ) was chosen for the sub-millimeter holes compared to a typical diameter of 0.05–0.5mm for the MPP. In theory, it is possible to use a smaller hole diameter to get a better sound absorption performance at a particular frequency, while the requirements for small holes are likely to restrict peak absorption in a narrow frequency band within manufacturing constraints. In the present case, a broadband sound absorption in the band from 953 Hz and 2332 Hz is favored rather than a perfect absorption at a single frequency, so relatively larger holes could be used. Also, in practice, as the hole diameter becomes small, the hole drilling process becomes difficult and, therefore, expensive. Consequently, as a trade-off between sound absorption performance and machining cost, moderate holes of 0.8mm diameter are preferred in the current work. It should be noticed that the above analysis is purely analytic and has neglected the effect of fan structures (such as blades and shafts) on noise absorption. In the following section, a 3D numerical study with FEM will be used to investigate the acoustic response of the MPP casing in terms of sound absorption.

### 3.3 Numerical modeling of the MPP casing

To further improve the modeling accuracy, a 3D acoustic FEM simulation is performed using the acoustic module in COMSOL Multiphysics® [24]. Flow effects are included in the MPP impedance model, while the background mean flow is assumed to be negligible. Hence, the sound pressure  $p$  ( $\sim e^{i\omega t}$ ) will satisfy a generalized wave equation in the form of

$$\nabla \cdot \left( \frac{1}{\rho_0} (\nabla p - \mathbf{q}) \right) + \frac{k^2 p}{\rho_0} = 0, \quad (4)$$

where  $\mathbf{q}$  is a dipole source corresponding to a volumetric domain force ( $\text{N/m}^3$ ), which here is put to unity for each blade to simulate the acoustic source produced by the fluctuating forces. The direction of the dipole is normal to the blade orientation. The dipole location is set to be at 85% blade span and close to the trailing edge for the front rotor blade, while it is close to the leading edge but at the same blade span for the rear rotor blade [25-27].

The boundary conditions employed in the study include sound hard-wall boundary, given by

$$-\mathbf{n} \cdot \mathbf{u} = 0 \quad (5a)$$

and acoustic impedance boundary in the form of

$$-\mathbf{n} \cdot \mathbf{u} = -p / Z \quad (5b)$$

where  $\mathbf{n}$  is the unit normal pointing into the fluid,  $\mathbf{u}$  is the acoustic velocity, and  $Z$  is the impedance. It is clear that when  $Z$  approaches infinite, Eq. (5b) becomes Eq. (5a), and that both equations ensure the continuity of normal velocity on the boundary without considering mean flow effects.

The computational domain, as well as the FEM mesh, is illustrated in Fig. 3. The global maximum element size is set equal to the minimal wavelength divided by 5, that is,  $\lambda_{min}/5 = 22.7\text{mm}$ , which corresponds to a maximum frequency of 3000 Hz used in the simulation. The mesh elements are clustered near the blade leading edges, the dipoles, and the hub fillets in order to capture the detailed features of the CR fan structures. Additionally, the swept mesh technique is utilized inside the perfectly matched layer (PML) with 6 elements throughout the layer thickness (0.1m). An inboard radiation sphere of diameter 0.5m is surrounded by the PML and centers at the origin of duct inlet. Likewise, the duct outlet is set to be PML. The hubs and blades of the CR fan are modeled as rigid bodies, so the sound hard wall boundary condition is applied on their surfaces. In total, there are almost 1.4 million mesh elements and 2.2 million degrees of freedom (DOFs) to be solved in the FEM simulations.

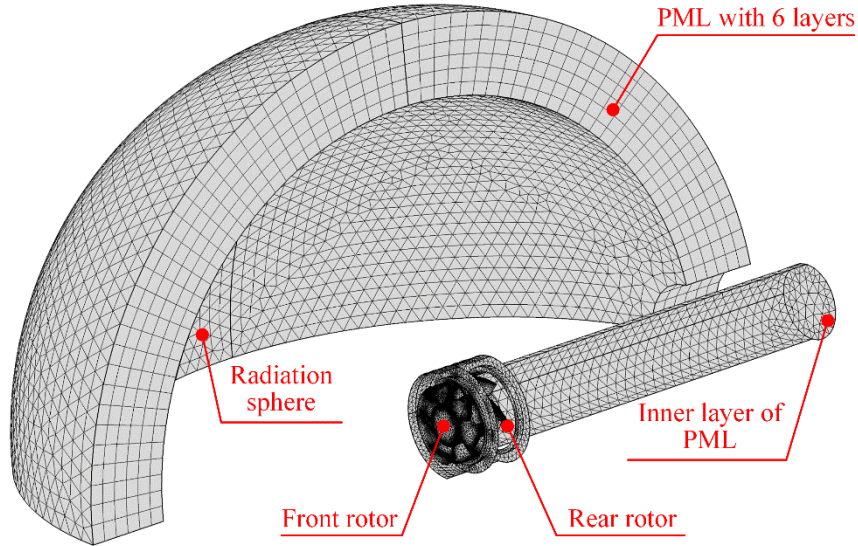


Fig. 3. The computational domain and mesh in COMSOL.

The sound intensity  $I$  is averaged over the front or intake hemisphere of the radiation domain at each frequency, which is determined as

$$\bar{I} = \frac{\iint_S I dA}{S}, \quad (6)$$

where  $S$  is the surface area of the intake hemisphere. The intake fan noise reduction  $\Delta B$  (in dB or dBA) using microperforated casing treatments can, therefore, be defined as

$$\Delta B = 10 \log_{10} \left( \frac{\bar{I}_h}{\bar{I}_m} \right), \quad (7)$$

where  $\bar{I}_m$  and  $\bar{I}_h$  denote the averaged intensity with and without MPP casing treatments, respectively. In numerical modeling, the configurations of installing the treatments over the front and rear rotors are studied. The hard-wall treatment, that is, without using the MPP casing treatment, is chosen as the baseline configuration for comparison.

Figure 4 demonstrates the result of the parametric frequency study from 120 Hz to 3000 Hz. Three treatment configurations have been numerically studied, which are Config. 2 (using the MPP casing over the front rotor), Config. 3 (Config. 2 with an enlarged back cavity) and Config. 4 (using the MPP casing over the rear rotor). In the figure, the open cavity is represented by a hollow rectangle and the closed one by a filled rectangle. Their acoustic benefits are denoted as black solid ( $\text{—}$ ), blue dot-dashed ( $\text{--}\cdot\text{--}$ ), and green dashed ( $\text{--}\cdot\text{--}$ ) curves, respectively. Note that the result of the baseline configuration without treatment is indicated as a zero-benefit line in the figure (the red dotted line  $\text{...}$ ).

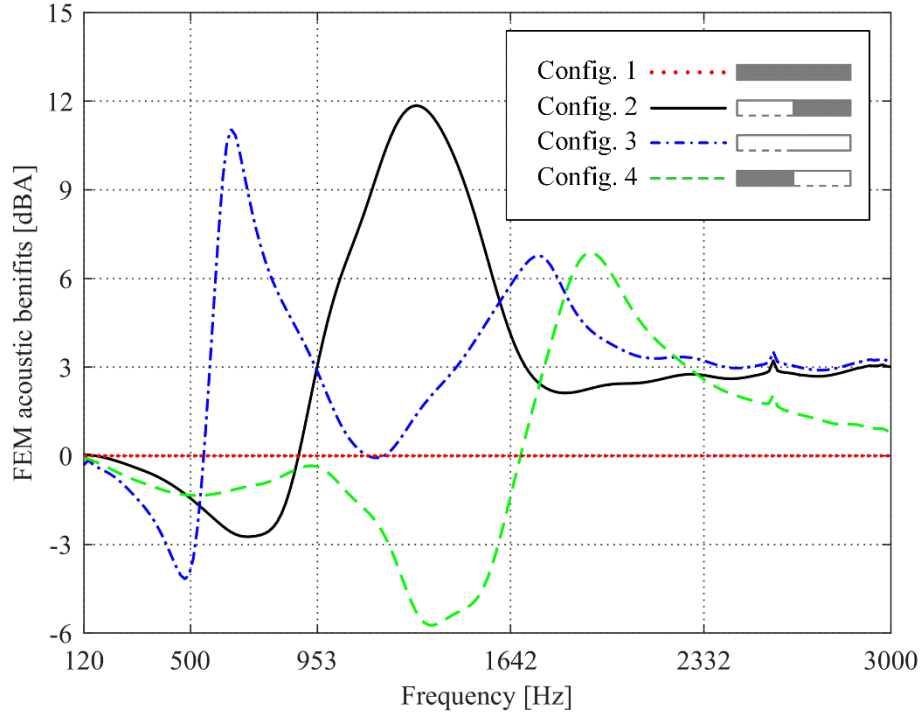


Fig. 4. FEM acoustic benefits obtained using the MPP casing treatments.

The configurations of installing the treatments over the fan rotor will be documented systematically in § 4. In general, the case of incorporating the MPP treatment over the front rotor outperforms the case with the treatment over the rear rotor. The main peaks of Configs. 2 and 3 are approximately 5 dBA higher than that of Config. 4. It is interesting to note that there are two peaks in the curve of Config. 3, of which one is at a lower frequency of 650 Hz and the other at a higher frequency of 1740 Hz. Meanwhile, the peak absorption of Config. 2 (with a regular back cavity) is moved to a lower frequency (1350 Hz) compared to that (1750 Hz) determined by Eqs (2) and (3), which is believed to be caused by fan structures and oblique incidence of sound wave. For each configuration, it has a frequency range starting from 120 Hz where the MPP treatment is found to increase sound radiation by the dipole sources. As far as Configs. 2 and 3 are concerned, their ineffective frequency ranges extend to 900 Hz and 550 Hz, respectively. After that, substantial noise reductions can be found for both configurations. In particular, Config. 4 has a better acoustic performance at lower frequencies between 550 Hz and 950 Hz and at higher frequencies above 1600 Hz, while Config. 2 is more effective in the mid-frequency range between 950 Hz and 1600 Hz. In contrast, it is not until 1680 Hz that some attenuations can be observed for Config. 4, and its peak absorption happens at a much higher frequency of 1930 Hz than those

of Configs. 2 and 3. In addition, there is an evident dip presented in the curve starting from 950 Hz with a width of 720 Hz and a depth of 6 dBA, which is more noticeable compared to those of Configs. 2 and 3. As a whole, the numerical results demonstrate that installing the MPP casing over the rear rotor of CR fans is not an effective way to control intake fan noise. Note that, although the positions of peak absorption do not coincide with the tone at 1642 Hz exactly, both Configs. 2 and 3 are still able to attenuate this tone by up to 6 dBA, and they are also acoustically effective in the predefined frequency range from 953 Hz to 2332 Hz. Hence, the acoustic parameters defined in §3.2 are reasonable, arriving at a satisfactory compromise between acoustic performance, manufacturing cost, and fan-structure constraints.

### 3.4 Interaction between MPP casing and fan rotor

The sub-millimeter holes of the designed casing are evenly distributed in the axial and circumferential directions, as illustrated in Fig. 5. Each row of holes in the axial direction behaves like a stator vane, interacting with the rotor blades as they sweep across the row in the circumferential path. In essence, the casing-rotor interaction frequency and mode order can be defined based on the theory of stator-rotor interaction [17, 28, 29], as

$$f_{in} = \frac{1}{60} |nB\Omega| \quad \text{and} \quad m = nB - qV, \quad (8a, b)$$

where  $n$  and  $q$  are integers taking values from  $-\infty$  to  $+\infty$ , and  $V$  is the number of rows in the circumferential direction.

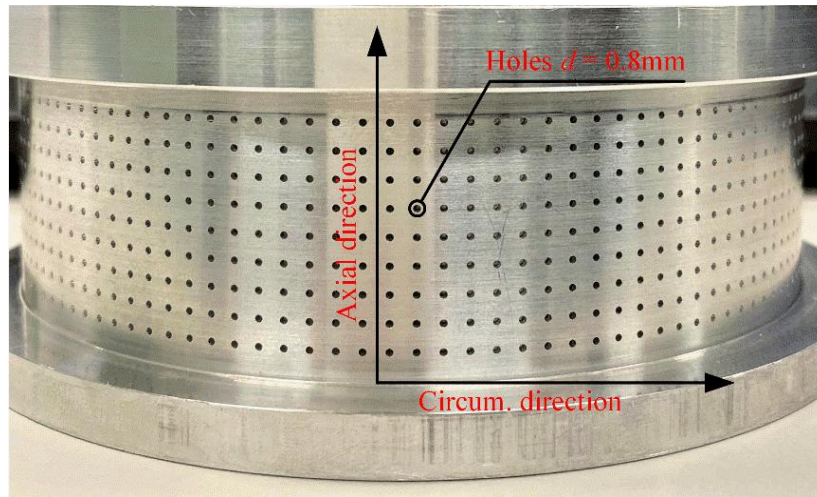


Fig. 5. The sub-millimeter holes in axial and circumferential (Circum.) directions.



As for the front rotor,  $B = B_1$  and  $\Omega = \Omega_1$ , and for the rear rotor  $B = B_2$  and  $\Omega = \Omega_2$ . The mode order  $m$  determines the radiation efficiency of the interaction tone through the Bessel function of the first kind,  $J_m(z)$ , where the argument  $z$  is equal to the radial wavenumber  $\kappa$  multiplied by the radius,  $r \in [r_h, r_t]$ . The radial wavenumber  $\kappa$  scales with the wavenumber of the interaction frequency,  $\kappa \sim 2\pi f_{in}/c_0$  [30]. As  $m$  approaches  $\infty$ , the Bessel function vanishes rapidly, suggesting that the interaction tone would become remarkable when  $m$  is small. As a consequence, the most efficient mode is the zeroth-order,  $m = 0$ , which should be carefully avoided when choosing the row number of holes in the design stage of the MPP casing.

In this paper, after defining the hole diameter  $d$  and the perforation ratio  $\sigma$ , we take the row number  $V = 123$  for the front casing and  $V = 127$  for the rear casing, producing interaction mode order  $m = 18 \times 7 - 1 \times 123 = 3$  at an interaction frequency of 7655 Hz ( $18f_1$ ), and  $m = 25 \times 5 - 1 \times 127 = -2$  at 6594 Hz ( $25f_2$ ), respectively. As can be seen, both arrangements ensure that if there is any significant casing-rotor interaction, it will occur at a higher frequency (beneficial to sound absorption) with a relatively higher order (poor at noise radiation). This is intended for minimizing the undesired effects of casing-rotor interaction. Figure 6 shows the 1/48 octave band spectrum of a case that failed to meet the requirement for the mode order  $m$ , thereby producing a loud interaction tone.

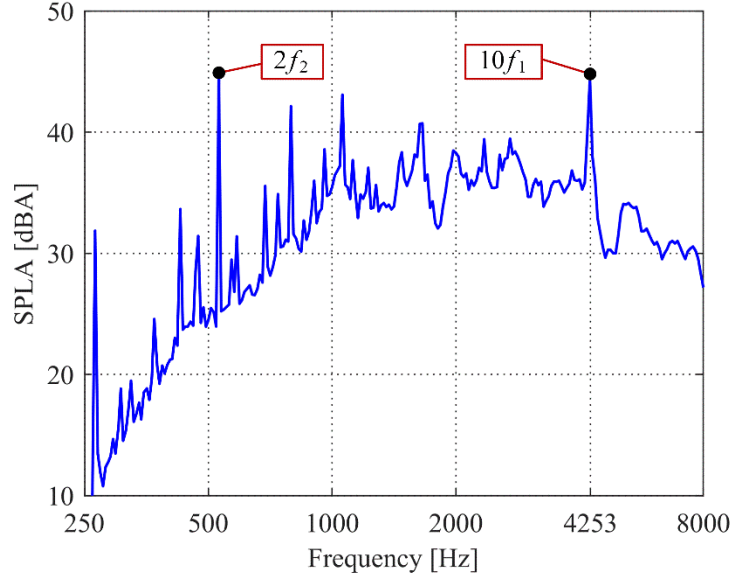


Fig. 6. The casing-rotor interaction tone at 4253 Hz ( $10f_1$ ).

In this case, the MPP treatment was placed over the front rotor of the CR fan, and the acoustic parameters were the same as stated in §§ 3.2 except for hole diameter  $d = 1.5\text{mm}$ . Note that, for the experiments conducted in the early stages, a series of relatively big holes were adopted, since the MPP was built using a rapid prototyping technique that was not appropriate for sub-millimeter structures. To get a perforation ratio of 4.95%, the row number  $V$  was coincidentally set to be  $V = 70$ . As a result, the mode order is defined as  $m = 10 \times 7 - 1 \times 70 = 0$ , and the interaction frequency is 4253 Hz ( $10f_1$ ), which has been marked in the figure. The noise level of this tone was found to be 40.4 dBA, being just 1.9 dBA lower than that of the most influential tone at 528 Hz ( $2f_2$ ). For better performance of noise reduction, the casing-rotor interaction tone must be eliminated in practice by adjusting the row number  $V$  of holes in the circumferential direction after determining the MPP acoustic parameters.

#### 4 The testing configurations

The casing treatments are tested in two axial locations; one is over the front rotor, and the other over the rear rotor, as indicated by two yellow rectangles in Fig. 7. The MPP casing over the rear rotor is 4mm longer than that over the front rotor in the axial direction. Both the casings are machined aluminum. Note that, by switching the channel on or off, the two cavities can be either connected or disconnected in order to regulate the volume of each cavity, which is intended for adjusting the cavity stiffness and, in turn, changing the resonance frequency of peak absorption. In total, there are 5 configurations to be investigated, as demonstrated in Table 2.

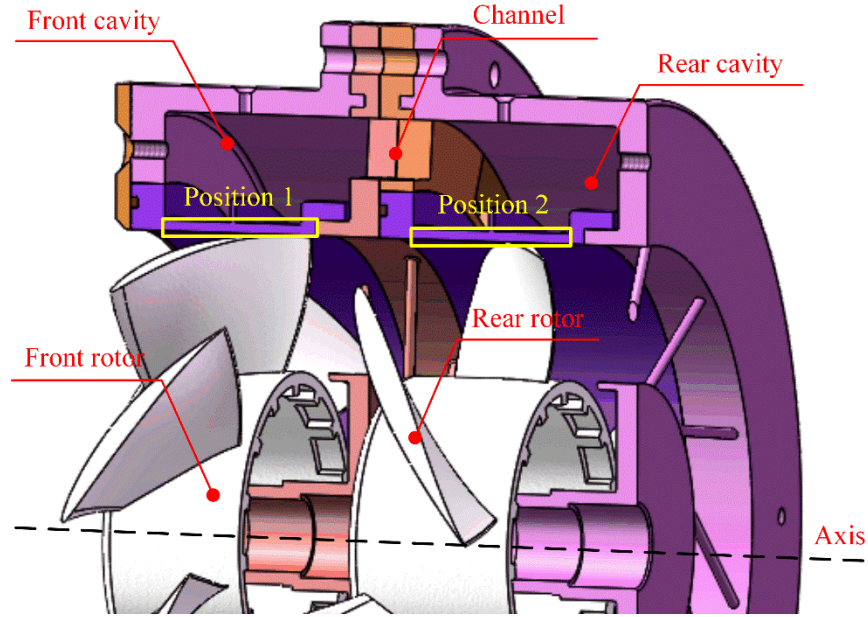


Fig. 7. The schematic of installing the MPP casing treatments over fan rotors.

In the rest of this paper, both the front and rear MPP casing treatments are designated using a series of digits following the abbreviations of FC and RC, respectively. The digits describe the arrangement of holes in the axial and circumferential directions. In this way, the front casing is denoted as FC1238 and the rear one as RC1279. The three digits in the middle represent the row number of holes around the circumference, and the fourth digit indicates the number of holes in the axial direction for each row. In particular, for a hard-wall casing, the 4 digits are made as zeroes, i.e., FC0000 and RC0000. The hard-wall treatment Config. 1 is selected as the baseline for aerodynamic and acoustic comparisons in the experiments.

**Table 2.** The testing configurations (Configs.) for data acquisition.

<i>Configs. MPP &amp; Cavity</i>	<i>Config. 1</i>	<i>Config. 2</i>	<i>Config. 3</i>	<i>Config. 4</i>	<i>Config. 5</i>
FC0000	<b>Yes</b>	No	No	No	No
FC1238	No	<b>Yes</b>	<b>Yes</b>	No	No
RC0000	<b>Yes</b>	No	No	No	No
RC1279	No	No	No	<b>Yes</b>	<b>Yes</b>
Cavity connected	No	No	<b>Yes</b>	No	<b>Yes</b>

## 5 Results from CR fan testing

### 5.1 MPP casing treatment over the front rotor

The fan total pressure rise ( $\Delta P$ ) and the overall noise level of Configs. 1, 2, and 3 are presented in Figs. 8a and 8b as a function of the volumetric flow rate ( $Q$ ), respectively. Both figures have the same line fonts. Figure 8a shows that including the MPP casing treatment (FC1238) over the front rotor has negligible influences on the fan aerodynamic performance except in the region of extremely low or high flow rate, where a pressure loss of 6-10 Pa can be found compared with the baseline configuration (Config. 1). Furthermore, switching the channel between cavities off or on does not make a difference in fan performance throughout the flow rate region of consideration.

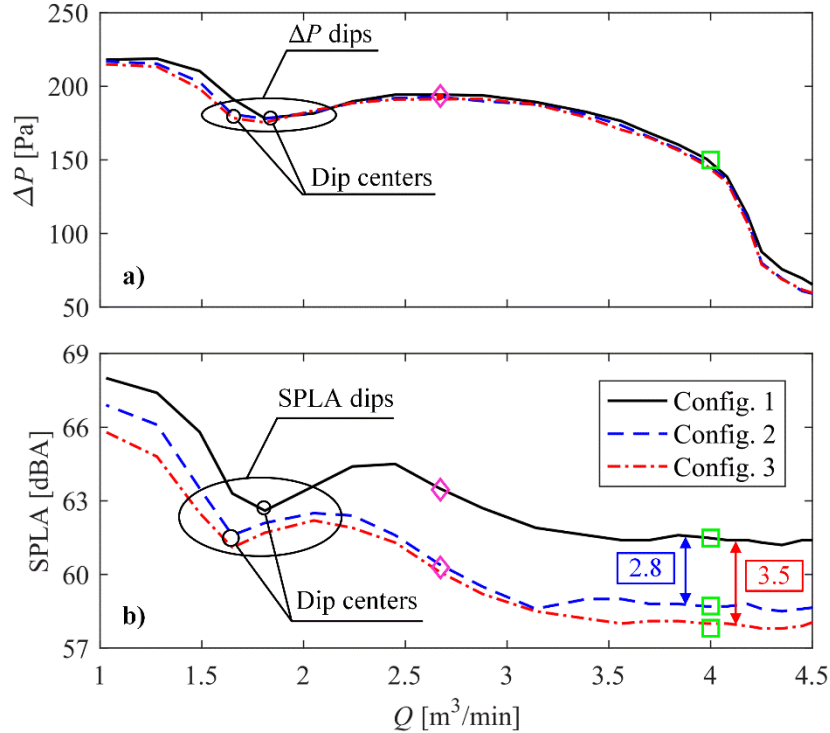



Fig. 8. The variation trends of a) pressure rise and b) noise level for Configs. 1 to 3.

Figure 8b shows a similar variation trend of overall noise for Configs. 1, 2, and 3. In general, to the right of the stall inception points (marked by magenta diamonds  $\diamond$ ), the overall noise levels are lower and do not change much all the way to the free delivery condition, but the drops of total pressure become increasingly rapid, especially beyond the fan design point. In Fig. 8a, in the flow rate region below stall inception, the pressure curves first show a slight increase and then enter a characteristic dip before climbing up to the left. On the other hand, the noise level curves in Fig. 8b show a similar variation trend.

8b experience resemblant dips before starting to grow again in the region of extremely low flow rate. For each configuration, the regions of pressure dip and noise level dip coincide with each other, as indicated in Figs. 8a and 8b. However, it should be noted that the MPP treatments tend to move the dip centers of their respective curves slightly to the left and thus into a lower flow rate region, implying a delayed stall. In experiments, the CR fan was found to operate in an unstable state in the region below stall inception, where a louder noise could be heard compared to that around the design point.

In general, incorporating the MPP casing treatment over the front rotor is able to attenuate overall noise throughout the flow rate region, while Config. 3 with an enlarged cavity has a better performance in noise reduction than that of Config. 2. More specifically, in the flow rate region above stall inception, an overall noise reduction of 3.5 dBA can be attained with Config. 3 compared to 2.8 dBA with Config. 1. In the region between stall inception and the center of the dips, both configurations are subject to a rapidly deteriorating performance in noise reduction. It is worth mentioning that near the dip center of the baseline curve, noise reductions are the lowest and not more than 1 dBA. After that, however, the acoustic benefits recover gradually, and Config. 3 can attenuate noise by up to 2.6 dBA, being averagely 1 dBA higher than that of Config. 2. In the following, spectral analysis concerning the fan working at the design point (denoted by green squares ) will be carried out. Also, noise reductions at the prominent tones will be reported. For Configs. 1, 2, and 3, the averaged and SCP spectra at the design point are presented in Figs. 9a and 9b, respectively. Both figures use the same line fonts. For the prominent tones, acoustic benefits achieved by Configs. 2 and 3 are given in Table 3. It is worth noting that there are no peaks or steps occurring at 7655 Hz, meaning that the casing-rotor interaction has been restrained.

**Table 3.** Acoustic benefits achieved at the prominent tones with Configs. 2 and 3.

<b>Frequency</b> <b><math>f_{in}</math> (Hz)</b>	$2f_2$ 528	$f_1+f_2$ 690	$3f_2$ 792	$f_1+2f_2$ 953	$2f_1+3f_2$ 1642	$3f_1+4f_2$ 2332
<i>Config. 2</i>						
<b>SPLA (dBA)</b>	41.9	34.7	40.8	33.4	31.3	35.9
<b>Benefits (dBA)</b>	-1.1	1.2	-3.0	6.5	11.3	2.7
<i>Config. 3</i>						
<b>SPLA (dBA)</b>	39.2	28.1	28.0	30.8	33.8	32.3
<b>Benefits (dBA)</b>	1.6	7.8	9.8	9.1	8.8	6.3

In Figs. 9a and 9b, the curves are almost overlapped below 528 Hz, indicating that the acoustic energy contained in this range does not change much. For the tone at 528 Hz, Config. 2 with

channel switched-off tends to increase noise level by 1.1 dBA (indicated as a minus value in Table 3). In contrast, only a limited attenuation of 1.6 dBA is obtained by Config. 3. Recall that Config. 3 has a better performance at lower frequencies compared with Config. 2 due to an enlarged cavity (refer to Fig. 4).

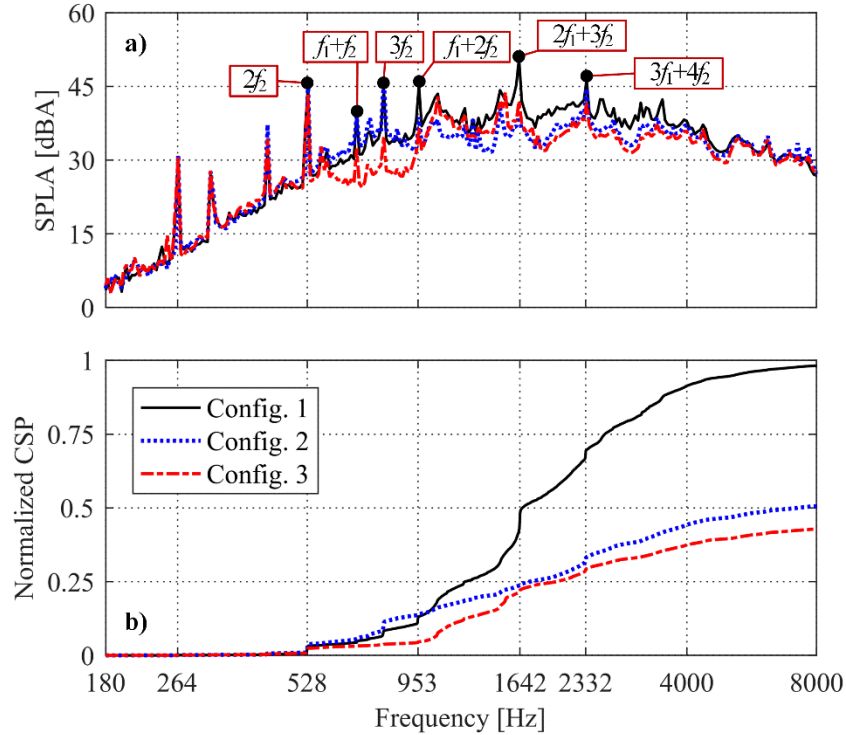


Fig. 9. The comparison of noise spectra from the CR fan treated with FC1238;

a) the averaged spectrum and b) the normalized CSP spectrum.

Besides, Figs. 9a and 9b show that the curves of Config. 3 are much lower than those of Config. 1, while those of Config. 2 are the highest from 528 Hz to 953 Hz. It is therefore implied that broadband noise therein can be reduced using Config. 3, while it is slightly boosted by Config. 2, which agrees with the FEM simulations. As seen in Table 3, both configurations are able to attenuate interaction tones at 690 Hz and 953 Hz, but Config. 3 is also effective for the rotor-alone tone at 792 Hz, where Config. 2 fails, and thus an increase of 3 dBA can be noticed. It is speculated that this ineffectiveness is due to increased turbulence caused by perforations. As these turbulence structures are conveyed downstream by the mean flow, they will be chopped periodically by the rear rotor blades, thus radiating more noise at rotor-alone tones of 528 Hz and 792 Hz. Meanwhile, Config. 2 is not acoustically effective below 900 Hz based on the FEM simulations, so both tones cannot be attenuated but strengthened. However, beyond 953 Hz, the curve of Config. 2 in Fig. 9a

becomes the lowest until 1642 Hz, suggesting a better performance of reducing noise compared to Config. 3, which is also consistent with the FEM simulations. In Table 3, it is demonstrated that both Configs. 2 and 3 are able to attenuate the tone at 1642 by more than 8 dBA, thereby eliminating the corresponding vertical step in the SCP spectra, as shown in Fig. 9b.

Figure 9a demonstrates that the spectral curves of Configs. 2 and 3 are close to each other and also relatively lower than that of Config. 1 above 1642 Hz. Therefore, moderate noise reductions can be obtained, while Config. 3 performs comparatively better than Config. 2. This is because the former has a better response at higher frequencies (see Fig. 4). In the band from 953 Hz to 2332 Hz, the portion of acoustic energy contained drops dramatically from 60% to 23% for Config. 2 and to 24% Config. 3. Furthermore, the opening between the baseline curve and the curve of either Configs. 2 or 3 presents no tendency to narrow even beyond 2332 Hz, which indicates that both configurations are also able to attenuate noise in the high-frequency range. In particular, at 2332 Hz, Configs. 2 and 3 gain noise reductions of 2.7 dBA and 6.3 dBA, respectively (see Table 3). At 8000 Hz, the normalized cumulative power decreases to 51% for Config. 2 and 43% for Config. 3, which corresponds to 2.8 dBA and 3.5 dBA reductions of overall noise, respectively.

For better comparison, acoustic benefits achieved in experiments and simulations are further replotted in a scale of 1/3 octave band from 160 Hz to 2500 Hz, as shown in Fig. 10. The simulated benefit and its variation trends as a function of frequency agree well with the experimental results for Config. 3 (with an enlarged cavity). However, for Config. 2 the difference in the frequency band around 1260 Hz is more perceivable. This frequency is about three times the front rotor BPF (that is  $1260 \text{ Hz} \approx 3f_1$ ). As the blade tip under the MPP face sheet sweeps across the nearby row of holes, a jet flow is formed between the tip-clearance region and the back cavity of the MPP. The formation of such a jet flow happens at the front rotor BPF and its harmonics, where the MPP sound absorption performance is likely to deteriorate. This may explain why a relatively big difference between numerical and experimental benefits can be noticed around 1260 Hz since the COMSOL model cannot predict the complex jet flow through the holes. In spite of the difference around 1260 Hz, the trends are generally in agreement. It is therefore concluded that the numerical modeling (refer to §§ 3.2) in terms of designing MPP casing treatments is generally valid to characterize their acoustic performance in fan noise reduction.

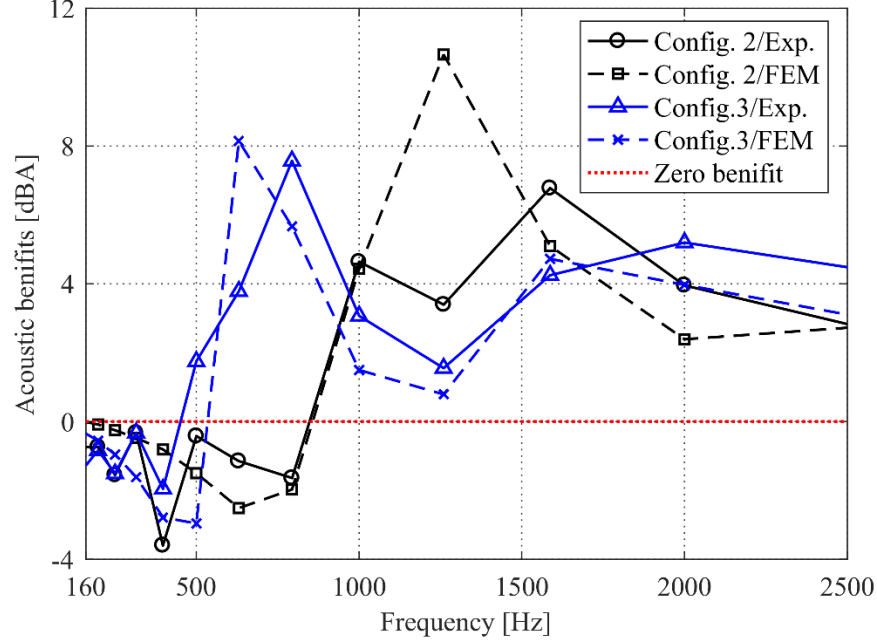


Fig. 10. The comparison between numerical and experimental (Exp.) benefits for Configs. 2 and 3.

Base on the above analyses, the front MPP casing (FC1238) with connected cavities (Config. 3) can make more contributions of attenuating noise at all the prominent tones except for the one at 1642 Hz, where Config. 2 is, however, more effective. On the whole, Config. 3 has better performance. The acoustic benefits achieved through the insertion of the MPP casing over the front rotor can be attributed to the combination of sound absorption and flowfield modification in the blade tip region. As the noise from the rear rotor propagates around the MPP casing treatment, a traditional acoustic absorption can happen, and simultaneously the flowfield near the front blade tip is modified positively so that the wake-rotor and tip-vortex interactions are relieved, thereby reducing both tonal and broadband noise radiation in the far-field. This is why the broadband bottom (recall Fig. 9a) is lowered in a specific frequency range when using the casing treatment. However, in the frequency range where the MPP casing fails to attenuate noise (see Figs. 4 and 10), the mechanism of flowfield modification is believed to be more profound. To be specific, the fluid in the blade tip region is capable of migrating through perforations in the circumferential and axial directions, which would increase the local turbulence level. The turbulent structures will be ingested and chopped periodically by the rear rotor, radiating more noise at rotor-alone tones. These amplified tones from the rear rotor could be attenuated when propagating upstream by the casing treatment if it is effective at the corresponding frequencies. Such is the case with Config. 3.



## 5.2 MPP casing treatment over the rear rotor

The fan total pressure rise ( $\Delta P$ ) and the overall noise level of Configs. 4 and 5 are illustrated in Figs. 11a and 11b, respectively. For comparison, the curves of Config. 1 are also shown, and both figures have the same line fonts. In contrast to front casing treatments, the aerodynamic performance experiences a pressure loss of no more than 10 Pa around the fan design point. This can be explained as follows.

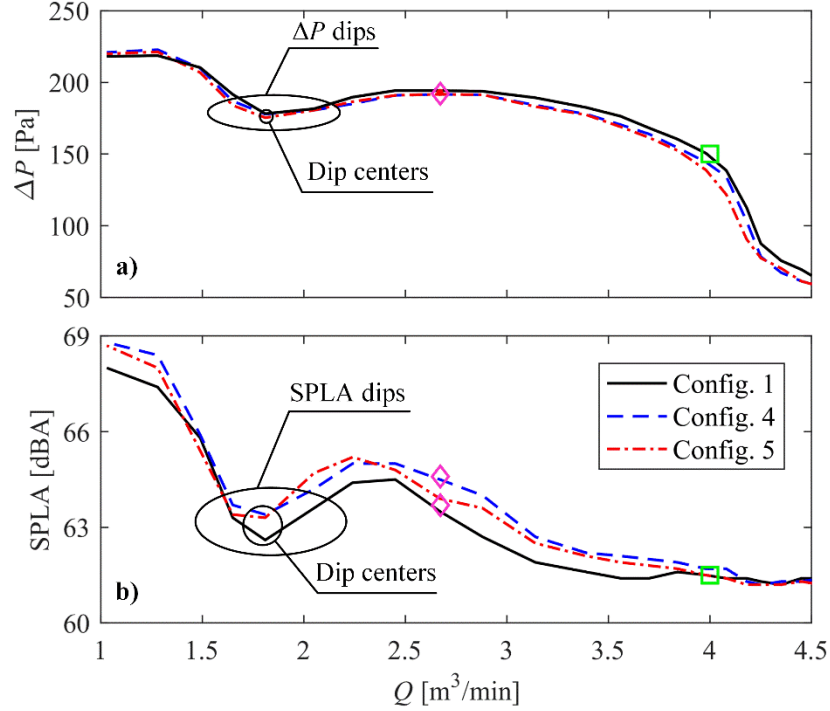


Fig. 11. The variation trends of a) pressure rise and b) noise level for Configs. 1, 4, and 5.

The environmental pressure over the rear rotor is higher than that over the front rotor, as the fluid into the CR fan is consecutively pressurized by the front and rear rotors. Therefore, it is true that perforations of the rear casing (RC1279) tend to consume more energy and thus give rise to more pressure loss compared with the front casing (FC1238) when the pressurized fluid flows through the perforations and past the MPP face sheet. This result is consistent with the experimental findings by Sutliff and Jones [8], who showed that the static and total pressures behind the rotor would slightly decrease when using acoustic liners over the rotor to attenuate fan noise. Figure 11a demonstrates that the pressure loss is more evident in the region above stall inception than in the region below stall inception. Figure 11b compares the overall noise level as a function of the flow rate. It seems that installing RC1279 over the rear rotor increases the overall

noise level slightly nearly throughout the flow rate region. Besides, the centers of the pressure dip and SPLA dip occur at the same flow rate of 1.81 m<sup>3</sup>/min without being shifted by the MPP treatments. In the below, spectral analysis of the testing fan working at the design point (marked by green squares  $\blacksquare$  in Fig. 11) will be given.

**Table 4.** Acoustic benefits achieved at the prominent tones with Configs. 4 and 5.

<b>Frequency <math>f_{in}</math> (Hz)</b>	$2f_2$ 528	$f_1+f_2$ 690	$3f_2$ 792	$f_1+2f_2$ 953	$2f_1+3f_2$ 1642	$3f_1+4f_2$ 2332
<i>Config. 4</i>						
<b>SPLA (dBA)</b>	37.6	34.0	38.0	29.5	34.6	39.1
<b>Benefits (dBA)</b>	3.2	1.9	-0.2	10.4	8.0	-0.5
<i>Config. 5</i>						
<b>SPLA (dBA)</b>	39.4	35.3	38.5	33.1	35.8	40.3
<b>Benefits (dBA)</b>	1.4	0.6	-0.6	6.8	6.8	-1.7

Figure 12a provides the comparison of the average spectra of Configs. 4 and 5 to that of the baseline configuration and Fig. 12b compares the CSP spectra. The acoustic benefits achieved at the prominent tones are shown in Table 4. It can be seen that there are no visible peaks or steps appearing at 6594 Hz, so the acoustic interaction between the MPP casing and the rear rotor is suppressed. In the frequency range below 953 Hz, there are no obvious acoustic benefits achieved in broadband noise by the rear casing treatments (RC1279). However, as shown in Table 4, moderate noise reductions can be obtained at 528 Hz and 690 Hz, where Config. 4 generates more benefits. For the rotor-alone tone at 792 Hz, both configurations are found to increase its noise level slightly. In contrast, significant noise reductions can be obtained for the interaction tone at 953 Hz, while Config. 4 performs better than Config. 5, giving an additional reduction of 3.6 dBA.

In the band between 953 Hz and 2332 Hz, Fig. 12a shows that the broadband bottoms of Configs. 4 and 5 are higher than that of Config. 1, meaning that the broadband noise therein is increased. This makes the curves of Configs. 4 and 5 climb up at a faster rate than that of Config. 1 in Fig. 12b. In spite of the increased broadband noise, the tonal noise level at 1642 Hz can be reduced by more than 6 dBA. For the tone at 2332 Hz, the noise level is, however, increased by 0.5 dBA and 1.7 dBA by Configs. 4 and 5, respectively. In the range above 2332 Hz, the CSP curves in Fig. 12b are close to each other and rise gradually, and no noise reductions can be found. Overall, at 8000 Hz, the normalized CSP remains the same for Config. 5, while it is marginally increased by 5% for Config. 4 compared to that of Config. 1. It is concluded that the increase in broadband noise counteracts noise attenuations achieved at the prominent tones by both

configurations. Therefore the overall noise level cannot be reduced. In other words, installing the MPP casing treatments over the rear rotor does not bring many benefits in terms of CR fan intake noise control, which is consistent with the FEM simulations.

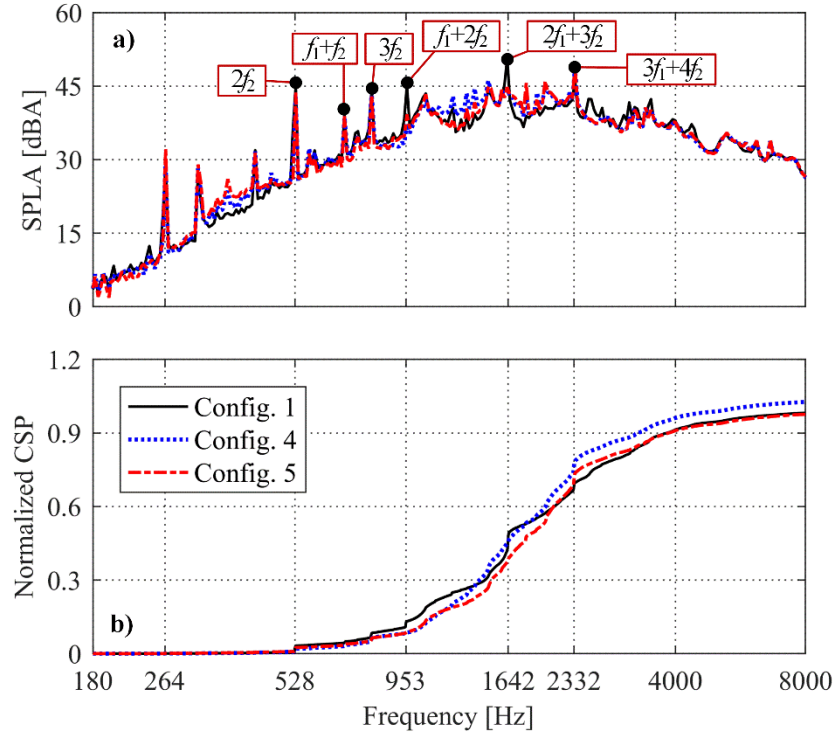


Fig. 12. The comparison of noise spectra from the CR fan treated with RC1279;  
a) the averaged spectrum and b) the normalized CSP spectrum.

Likewise, the experimental and numerical benefits are further replotted in a scale of 1/3 octave band, as can be seen in Fig. 13. Note that the comparison is made only for Config. 4, since Config. 5 presents a similar result. As shown in the figure, both the curves are close to the zero-benefit line (that is, the red dotted line  $\cdots$ ), except in the octave band centering around 2000 Hz, where a relatively big difference can be perceived between experimental and FEM benefits. This could arise from the flow effects induced by the MPP casing, which cannot be included in the FEM simulations. Despite such a difference, both the FEM and experimental results show that Config. 4 can obtain limited or barely no acoustic benefits.

In essence, the rear rotor is a significant contributor to interaction noise due to the wake-rotor and tip-vortex interactions. The upstream wakes and tip leakage vortices, rotating at an angular velocity of  $\Omega_1$ , are chopped by the rear rotor blades, thereby radiating noise at interaction

frequencies. In the meanwhile, rotor-alone tones can be produced by the interaction between upstream turbulent structures and the rear rotor.

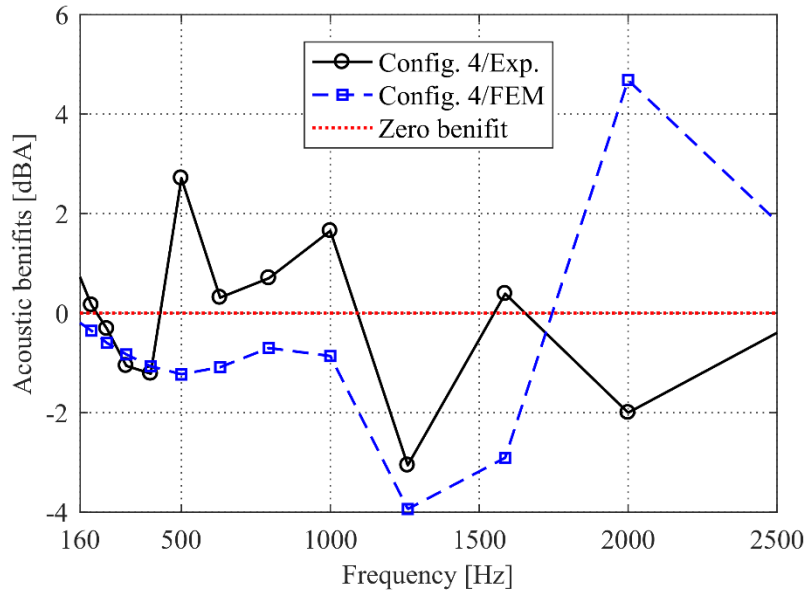


Fig. 13. The comparison between numerical and experimental (Exp.) benefits for Config. 4.

The flowfield in the rear rotor tip region is modified due to the inclusion of the rear casing treatment (RC1279), which will, in turn, change the rear rotor response to the wake-rotor interaction and especially the tip-vortex interaction, as the treatment is in close vicinity to the blade tip. Note that the rear casing is intended to change the response rather than the interaction itself, which is different from the effects of the front MPP casing treatment (FC1238). Such a modified response to the upstream wakes and vortices favors noise attenuations at some tones but may induce more noise at other ones (recall Table 4). Meanwhile, as has already been said, the MPP perforations could change the turbulence intensity and scale in the blade tip region, which may increase broadband noise in some frequency band (see Fig. 12). In fact, the fluid in the blade tip region is able to migrate circumferentially and axially through holes (refer to Fig. 3) due to pressure differences, that is, from the pressure to the suction side and from the downstream to the upstream location of the blade. It is speculated that an enlarged volume of the cavity would facilitate these migrations through perforations and thus induce more interferences on rear rotor blades. However, its acoustic impacts on overall noise are not obvious. Moreover, the swirling flow from the front rotor is likely to channel the acoustic pressure away from the impedance surface over the rear rotor, which would render the rear MPP casing ineffective [1, 31]. In conclusion, the combined experimental and simulation analysis suggests that the effects of placing the MPP casing treatment

over the rear rotor are more related to source modification rather than sound absorption. In practice, it seems to be an invalid strategy of reducing CR fan intake noise with MPP casing treatments over the rear rotor, in that the most prominent wake-rotor and tip-vortex interactions between rotors are hardly modified both directly and positively. It is, however, possible that such treatments are more beneficial to exhaust noise control of CR fans, which is left to future research.

## 6 Conclusions

The quest for a quiet environment has led to numerous efforts to combat fan noise, and acoustic performance is becoming one of the major indices differentiating one fan manufacturer from another for a broad range of consumer products where small-sized fans are used. In general, industrial fan manufacturers prefer to adopt an already developed and proven noise reduction method for fan noise control. In this regard, the microperforated-panel (MPP) liner is particularly useful and robust even in some harsh environments where dust, moisture, or temperature changes could be a problem for porous absorption since the MPP can provide clear sound absorption without the need for fiberglass or other porous materials. In the current study, for a small-sized contra-rotating (CR) fan, the effects of installing MPP casing treatments over the rotor on fan noise reduction and aerodynamic performance have been investigated. The research work of this study is expected to be helpful for industrial fan manufacturers in developing quieter small-sized CR fans integrated with MPP casing treatments. The conclusions are made as follows.

1. The acoustic parameters of the MPP casing were determined based on the spectral knowledge of the CR fan working at the design point and simulated with the finite element method (FEM), which showed that configurations of placing the treatment over the front rotor were more acoustically effective than those over the rear rotor. More importantly, it was found in experiments that the acoustic interaction between the rotor blade and each axial row of holes of the MPP behaves like the stator-rotor interaction, generating modes of order  $m = nB - qV$  at frequencies  $f_{in} = nB\Omega$ . Such interaction is likely to induce loud tones and therefore needs to be suppressed by optimizing the row numbers in an effort to increase mode orders  $m$  and frequencies  $f_{in}$ . This interaction phenomenon has not been clearly pointed out in previous literature.

2. In the flow rate region around the CR fan design point, the aerodynamic penalties were insignificant for the MPP casing treatment over the front rotor. In contrast, a pressure loss of no more than 10 Pa was observed with the treatment over the rear rotor. All the treatment configurations presented similar pressure dips and noise level dips in the flow rate region below stall inception, where the CR fan stalled, and thus, a louder noise would be heard compared to that around the design point.
3. The acoustic performance of the MPP casing treatment over the front rotor was excellent, attenuating overall noise throughout the flow rate region. In general, more acoustic benefits could be achieved in the higher flow rate region than in the lower flow rate region. Particularly around the fan design point, an overall noise reduction of up to 3.5 dBA was found with an enlarged back cavity behind the MPP face sheet, which was about 0.7 dBA higher than that obtained by the regular cavity. However, the overall noise level was slightly increased by the treatments over the rear rotor, and hence no acoustic benefits were achieved. Moreover, the treatment over the front rotor with an enlarged cavity was also able to attenuate all the interaction tones and rotor-alone tones with noise levels above 35 dBA. In contrast, the rest treatment configurations failed in noise reduction for some of these tones.

## **Acknowledgments**

The first author would like to acknowledge the support from China Aerodynamics Research and Development Center, and The University of Hong Kong. This work is also sponsored by the National Natural Science Foundation of China (NSFC, Grant No. 11972294).

## **References**

- [1] N. Peake, A.B. Parry, Modern challenges facing turbomachinery aeroacoustics, *Annu. Rev. Fluid Mech.* 44 (2012) 227-248.
- [2] C. Horvath, Beamforming investigation of dominant counter-rotating open rotor tonal and broadband noise sources, *AIAA J.* 53 (2015) 1602-1611.
- [3] B. Dong, C.Y. Jiang, X. Liu, Y. Deng, L.X. Huang, Theoretical characterization and modal directivity investigation of the interaction noise for a small contra-rotating fan, *Mech. Syst. Signal Proc.* 135 (2020) 106362.

- [4] E. Envia, Fan noise reduction: an overview, *Int. J. Aeroacoust.* 1 (2002) 43-64.
- [5] S. Bianchi, A. Corsini, A.G. Sheard, A critical review of passive noise control techniques in industrial fans, *J. Eng. Gas Turbo. Power* 136 (2014) 0440011-0440019.
- [6] C. Wang, L.X. Huang, Passive noise reduction for a contrarotating fan, *J. Turbomach.* 137 (2015) 0310071-03100710.
- [7] M.R. Khorrami, F. Li, M. Choudhari, Novel approach for reducing rotor tip-clearance-induced noise in turbofan engines, *AIAA J.* 40 (2002) 1518-1528.
- [8] D.L. Sutliff, M.G. Jones, Low-speed fan noise attenuation from a foam-metal liner, *J. Aircraft* 46 (2009) 1381-1394.
- [9] D.L. Sutliff, M.G. Jones, T.C. Hartley, High-speed turbofan noise reduction using foam-metal liner over-the-rotor, *J. Aircraft* 46 (2009) 1381-1394.
- [10] S. Allam, M. Abom, Fan noise control using microperforated splitter silencers, *J. Vib. Acoust.* 136 (2014) 0310171-0310178.
- [11] Q. Xi, Y. Choy, L. Chen, S. Tang, Noise control of dipole source by using microperforated panel housing, *J. Sound Vibrat.* 362 (2016) 39-55.
- [12] S. Lee, J.S. Bolton, Testing of axial fans with microperforated housings, *Noise Control Engr. J.* 64 (2016) 511-521.
- [13] Z.B. Zhang, Y.K. Chiang, Y.S. Choy, C.Q. Wang, Q. Xi, Noise control for a dipole sound source using micro-perforated panel housing integrated with a Herschel-Quincke tube, *Appl. Acoust.* 148 (2019) 202-211.
- [14] M.R. Gazella, T. Takakura, D.L. Sutliff, R. Bozak, B.J. Tester, Evaluating the acoustic benefits of over-the-rotor acoustic treatments installed on the advanced noise control fan, 23rd AIAA/CEAS Aeroacoustics Conference, 2017, Denver, Colorado, AIAA-2017-3872.
- [15] M.G. Jones, B.M. Howerton, Evaluation of novel liner concepts for fan and airframe noise reduction, 22nd AIAA/CEAS Aeroacoustics Conference, 2016, Lyon, France, AIAA-2016-2787.
- [16] S. Allam, M. Abom, A new type of muffler based on microperforated tubes, *J. Vib. Acoust.* 133 (2011) 0310051-0310058.
- [17] M.V. Lowson, Theoretical analysis of compressor noise, *J. Acoust. Soc. Am.* 47 (1970) 371-385.

- [18] C. Wang, L.X. Huang, Theoretical acoustic prediction of the aerodynamic interaction for contra-rotating fans, *AIAA J.* 56 (2018) 1855-1866.
- [19] C. Wang, L. Cheng, Sound absorption of a micro-perforated panel backed by an irregular-shaped cavity, *J. Acoust. Soc. Am.* 127 (2010) 238-246.
- [20] C. Wang, X. Liu, Investigation of the acoustic properties of corrugated micro-perforated panel backed by a rigid wall, *Mech. Syst. Signal Proc.* 140 (2020) 106699.
- [21] D.Y. Maa, Potential of microperforated panel absorber, *J. Acoust. Soc. Am.* 104 (1998) 2861-2866.
- [22] S. Allam, M. Abom, Experimental characterization of acoustic liners with extended reaction, 14th AIAA/CEAS Aeroacoustics Conference, 2008, Vancouver, British Columbia, Canada, AIAA 2008-3074.
- [23] T.J. Cox, P. D'Antonio, *Acoustic absorbers and diffusers: theory, design and application*, Spon Press, London, 2009.
- [24] COMSOL Multiphysics® ver. 5.3, Acoustics Module.
- [25] H.Z. Lu, L.X. Huang, R.M.C. So, J. Wang, A computational study of the interaction noise from a small axial-flow fan, *J. Acoust. Soc. Am.* 122 (2007) 1404-1415.
- [26] X. Mao, B. Liu, H. Zhao, Numerical analysis of the circumferential grooves casing treatment in a counter-rotating axial flow compressor, *Appl. Therm. Eng.* 130 (2018) 29-39.
- [27] G. Delattre, F. Falissard, Influence of torque ratio on counter-rotating open-rotor interaction noise, *AIAA J.* 53 (2015) 2726-2738.
- [28] M.E. Goldstein, *Aeroacoustics*, McGraw-Hill, Inc., United States of America, 1976.
- [29] W.K. Blake, *Mechanics of flow-induced sound and vibration, Volume 2 Complex flow-structure interactions*, Academic Press, Florida, 1986.
- [30] A. Sharma, H.N. Chen, Prediction of aerodynamic tonal noise from open rotors, *J. Sound Vib.* 332 (2013) 3832-3845.
- [31] A.J. Cooper, N. Peak, Upstream-radiated rotor-stator interaction noise in mean swirling flow, *J. Fluid Mech.* 523 (2005) 219-250.